Phonon transport and waveguiding in a phononic crystal made up of cylindrical dots on a thin homogeneous plate

Y. Pennec,[1,*] B. Djafari Rouhani,[1] H. Larabi,[1] A. Akjouj,[1] J. N. Gillet,[1] J. O. Vasseur,[1] and G. Thabet[2]
[1]*Institut d'Electronique de Microélectronique et de Nanotechnologie, UMR CNRS 8520, UFR de Physique, Cité Scientifique, 59652 Villeneuve d'Ascq Cedex, France*
[2]*SGI Silicon Graphics SA, 21 rue Albert Calmette, 78350 Jouy en Josas, Versailles, France*
(Received 9 June 2009; revised manuscript received 1 September 2009; published 13 October 2009)

We present a theoretical analysis of the phonon transport and guiding of acoustic waves in a phononic crystal made up of a square array of cylindrical dots, which is deposited on a thin homogeneous plate. With appropriate choice of the geometrical parameters, this structure can display several gaps, one of them being well below the Bragg gap. With the help of the finite difference time domain method, we calculate the transmission coefficient vs the frequency and demonstrate a good agreement with the dispersion curves. We show the possibility of guided modes inside an extended linear defect created either by removing one row of cylinders or by changing the height or the materials constituting the dots in a row. The wavelengths of the waves transmitted in the low-frequency gap are about ten times larger than the width of the waveguide. We discuss the transmittivity of each confined mode appearing in the band gap as well as the conversion in the polarization of the transmitted waves which can occur more or less significantly.

DOI: 10.1103/PhysRevB.80.144302 PACS number(s): 43.20.+g, 43.40.+s, 63.20.−e

I. INTRODUCTION

Phononic crystals are heterogeneous materials constituted by a periodical repetition of inclusions in a matrix background.[1] Associated with the possibility of absolute band gaps in their band structure,[2–5] these materials have found several potential applications, especially in the field of confinement, waveguiding, and filtering[6–10] as well as in the field of sound isolation.[11–16] In addition to bulk phononic crystals, recent works dealt with the study of surface modes of semi-infinite two-dimensional (2D) phononic crystals.[17–21] During the last few years, a great attention has been devoted to investigation of the dispersion curves of acoustic waves in a free or supported plate for one-dimensional[22–24] or 2D (Refs. 25–31) phononic crystals. They can operate at the wireless telecommunications frequencies (around 1 GHz) when the lattice parameter is in the micron range.[32–34] Recently, we proposed a new type of finite-thickness phononic crystals constituted by a periodic array of cylinders, which are deposited on a free standing homogeneous plate.[35] We investigated the acoustic-wave dispersion in this structure and unraveled the conditions for existence of absolute band gaps. We highlighted the possibility of a so-called "low-frequency gap," for frequencies well below the Bragg gap (where the wavelengths in all the constituent materials are much smaller than the phononic crystal period), if the geometrical parameters of the structure are chosen appropriately. At higher frequencies, one or more absolute band gaps appear whose number depends on the height of the cylinders. This structure was also studied independently by Wu *et al.*[36,37] However, the calculation of the transmission coefficient with the finite difference time domain (FDTD) method remained to be done.

From the calculation of both transmission coefficients and dispersion relations, the purpose of this paper is to study the waveguiding effects through different types of linear defects in this phononic crystal. Such waveguides are obtained either by removing a row of dots or by replacing in a row the materials or geometrical parameters of the dots. In each case, we present a detailed study of the confined modes, the transmitting and nontransmitting characters of the corresponding bands, and the possibility of polarization conversion, which could frequently occur. The flexibility of tailoring the acoustic properties of phononic crystals, especially those utilized for waveguide design, makes them particularly suitable for a wide range of applications from transducer technology to filtering and guidance of acoustic waves. Moreover, it should be also pointed out that knowledge and engineering of phononic band structures is also a necessary step to investigate heat transport in heterogeneous nanostructured materials[38,39] since the existence of gaps and/or flat bands prohibits the propagation of phonons in certain frequency ranges.

The paper is organized as follows. In Sec. II, we present the model of the perfect phononic crystal plate and FDTD method used for calculation of both dispersion curves and transmission spectra. In Sec. III, we investigate the transmission of an incident longitudinal mode S_0 through three kinds of geometrical waveguides obtained, respectively, by removing one row of cylinders (Sec. III A), changing the height of the cylinders (Sec. III B), and changing the nature of the dots in the guide (Sec. III C). The conclusions are given in Sec. IV.

II. MODEL AND METHOD OF CALCULATION

Figure 1(a) is a scheme of the phononic crystal which is studied in this paper, namely, a heterostructure made up of a square array of steel cylindrical dots of radius r and height h, deposited on a thin homogeneous plate of silicon. The z axis is assumed to be perpendicular to the plate and parallel to the cylinders. We define the lattice parameter a of the periodic array as equal to 1 μm and the filling factor β, given by $\beta=\pi r^2/a^2$, equal to 56.4%. The thickness of the plate is

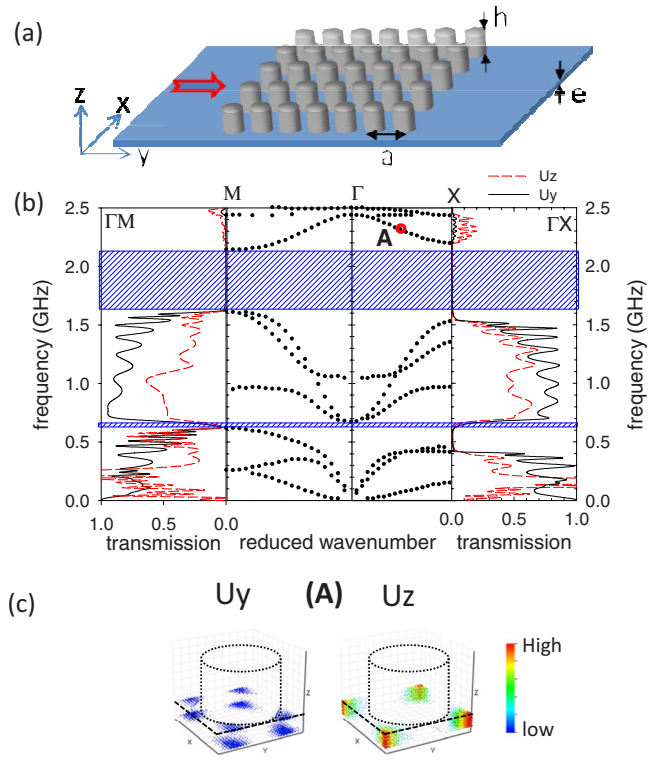

FIG. 1. (Color online) (a) Phononic crystal made of a square lattice of steel finite cylinders deposited on a homogeneous silicon plate. In our calculations, the length of the phononic crystal is ten periods. The geometrical parameters are $a=1$ μm, $h=0.6$ μm, and $e=0.2$ μm. The red arrow symbolizes the incident longitudinal pulse. (b) Middle: band structure calculated along the high-symmetry axes ΓX and ΓM of the Brillouin zone. From each side of the band diagram: transmitted curves of the longitudinal incident wave for the polarization U_y (black solid line) and for the polarization U_z (red dashed lines). The red (blue) area corresponds to the position of the low (high) absolute band gap. (c) Eigenmode calculation at the point A, defined by the coordinates ($ka/\pi=0.474$ and $f=2.312$ GHz). The blue (red) color corresponds to the lower (higher) value of the displacement field modulus while the white color corresponds to a displacement equal to zero but does not appears in the color bar.

denoted by e and takes the value $e=0.2$ μm. The materials composing the dots and plate are assumed to be of cubic symmetry with their crystallographic axes oriented along the coordinate axes x, y, and z. The elastic constants and mass densities of the materials involved in the calculations are given in Table I.

The FDTD method has been proven[12,40] to be an efficient method to obtain the dispersion curves and transmission spectra of phononic crystals. This method solves the elastic wave equations by discretizing time and space and replacing derivatives by finite differences. The space is discretized in x, y, and z directions using a mesh interval equal to $\Delta x=\Delta y=\Delta z=a/30$. The equations of elasticity are solved with a time integration step $\Delta t=\Delta x/(4c_l)$, where c_l is the highest velocity involving in the structure and number of time step usually equal to 2,[19] which is the necessary tested time for good convergence of the numerical calculations.

TABLE I. Physical characteristics of the used materials: ρ is the density and C_{11}, C_{12}, and C_{44} are the three independent elastic moduli of cubic structure.

Constant	Silicon	Steel	Aluminum
$\rho(\mathrm{kg/m^3})$	2331	7780	2730
$C_{11}(\mathrm{N/m^2})$	16.57×10^{10}	26.4×10^{10}	10.82×10^{10}
$C_{12}(\mathrm{N/m^2})$	6.39×10^{10}	10.2×10^{10}	5.12×10^{10}
$C_{44}(\mathrm{N/m^2})$	7.962×10^{10}	8.10×10^{10}	2.85×10^{10}

The dispersion curves were calculated using (i) a three-dimensional (3D) unit cell ($a.a.b$), which is repeated in the three spatial directions and (ii) the Bloch theorem, which introduces the wave vector $\boldsymbol{k}$. In the z direction, the length of the unit cell b is chosen so that the plate and cylinder as well as a thin layer of vacuum on both sides are embedded in order to decouple the interaction between neighboring cells. For each component of the wave vector (k_x and k_y) parallel to the plate, an initial random displacement is applied inside the unit cell at the origin of time. Then, the displacement field is recorded at many positions in the unit cell as a function of time and finally, Fourier transformed to obtain the eigenfrequencies of the structure for the chosen wave vector. Therefore, the band structures are computed in terms of frequency as a function of the wave vector and plotted along the principal directions of the 2D irreducible Brillouin zone (ΓXM).

The transmission spectra through perfect or defect-containing phononic structures were computed using a 3D FDTD code. Our calculation is performed in a 3D box with the propagation along the y axis. The box is finite along y and composed of a phononic crystal containing seven or ten cylinders, sandwiched between an ingoing and a outgoing media, which are two homogeneous plates of thickness e. Perfect matching layer (PML) conditions are applied at the boundaries of the box along the y direction. Along the x direction, the structure is periodic, which means that it contains one unit cell when dealing with a perfect phononic crystal. However, the waveguide is studied with a supercell of five periods to avoid the interaction between neighboring guides. Along z, a thin layer of vacuum is added on both sides of the phononic structure in order to decouple the interaction between repeating periodical cells. A broadband wave packet is initiated from the homogeneous plate in front of the phononic crystal. This wave is a longitudinal pulse, with a polarization and Gaussian profile along the y axis but uniform in the x and z directions. The transmitted signal is recorded as a function of time at the end of the perfect phononic crystal and integrated in the (x and z) plane for each component U_x, U_y, and U_z of the displacement field. For the waveguide structures, the throughput signal is integrated at the exit only over the cross section of the waveguide instead of the whole period in the x direction as it was the case for the perfect phononic crystals. We note that, with this procedure, the maximum value of the transmission can exceed the unity. Finally, the signals are Fourier transformed and normalized by an equivalent signal propagating through a single homogeneous silicon slab to yield the transmission coefficient. In practice, the U_x component vanishes so that

the transmission spectra will be obtained only for the U_y and U_z components.

For more efficiency, the code has been parallelized using message passing interface computation. The calculations were performed on an ALTIX XE 240 cluster from silicon graphics with 16 CPUs.

The band structure is presented in Fig. 1(b) in the frequency range [0 and 2.5 GHz] along the high-symmetry axes ΓX and ΓM of the first Brillouin zone. The choice of the geometrical parameters ensures the existence of two absolute band gaps extending, respectively, from 0.613 to 0.668 GHz and from 1.615 to 2.139 GHz. It should be noticed that at the frequency of the lowest band gap the wavelengths of the longitudinal and transverse waves in the silicon membrane are 13 and 9 times larger than the period of the phononic crystal. The higher gap appears in the Bragg frequency regime, where these wavelengths are about three or four times the lattice parameter. The origin and behavior of these gaps as a function of the geometrical and physical parameters of the whole structure have been already studied in a preceding paper.[35] Our first results, shown in the diagrams of Fig. 1(b), are the computing transmission spectra in the directions ΓX and ΓM of the Brillouin zone, which are displayed on each side of the central band diagram. In the transmission spectra, we differentiate the polarization U_y (black solid lines) and U_z (red dashed lines) of the detected signal. We can notice a good agreement between the transmission and dispersion curves and, in particular, the positions of the gaps. The number of Fabry-Perot oscillations appearing in the transmission spectra below 1.5 GHz is in accordance with the number of unit cells in the phononic crystal along the y direction. At frequencies above 2.1 GHz, we can observe an isolated branch with a negative slope which contributes to a transmission only for the polarization U_z normal to the plate while the detected signal for the component U_y is negligible. We made the calculation of one eigenmode along this branch, at the point A defined by the reduced wave number $ka/\pi=0.474$ and frequency $f=2.312$ GHz. This eigenmode, sketched in Fig. 1(c), presents a localization of the acoustic energy in the corners of the unit cell for the normal component U_z. In accordance with the polarization of this branch, the incident longitudinal mode has been partially converted into a normal polarized signal. This effect shows that an incident longitudinal symmetric pulse which is initiated inside the plate of thickness e can be partially converted into a transmitted signal perpendicular to the plate. Such property can be useful for the observation of the transmitted field with a laser interferometric technique, which is sensitive to the component of the displacement field normal to the plate.

III. LINEAR WAVEGUIDES

A. Conventional line-defect waveguide

The traditional way of creating a linear defect is to remove a row of dots. In our calculation, the length of the waveguide is assumed to be ten periods of the phononic crystal and the width of the waveguide, w_g, has been considered as a variable [Fig. 2(a)]. Figure 2(b) gives the transmission spectra for both components U_y and U_z of the displacement field through the waveguide with $w_g=1.2$ μm. As a comparison, we also give the transmission coefficient through the perfect crystal in red dashed lines. The shaded red and blue areas, respectively, represent the two band gaps. Increasing w_g from 0 to 1.2 μm leads to the emergence of transmitted signals in the gaps, the case of $w_g=1.2$ μm being presented in Fig. 2(b). Beyond this value, the number of confined modes in the band gaps increases too much, which is not most suitable for filtering or demultiplexing applications. Looking at Fig. 2(b), we observe a full transmission of the acoustic waves within the higher gap [1.615 and 2.139 GHz] for the U_y component while the U_z component remains weak. For the low-frequency gap [0.613 and 0.668 GHz], the opposite situation occurs, i.e., the transmitted signal has mainly an U_z component. The transmission coefficients in the pass band between the two gaps are also strongly perturbed by the presence of the waveguide.

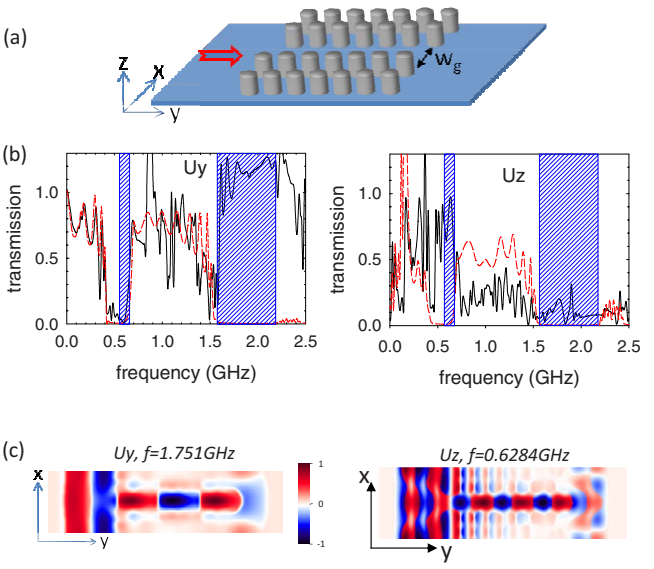

FIG. 2. (Color online) (a) Schematic view of a conventional line-defect waveguide; w_g corresponds to the adjustable waveguide width. The length of the phononic crystal is ten periods. (b) Black solid lines: transmission coefficient recorded at the exit of the waveguide for the polarizations U_y and U_z. Red dashed lines: transmission through the perfect phononic crystal structure. (c) Left: planar sections at the thickness $z=e/2$ of the displacement field distribution for the U_y polarization at the monochromatic frequency $f=1.751$ GHz. Right: same as previously for the polarization U_z and the monochromatic frequency $f=0.6284$ GHz. The red (blue) color represents the positive (negative) contribution of the wave.

To highlight the waveguiding properties through the gaps, the FDTD computation was used to simulate a monochromatic source, first at the frequency $f=1.751$ GHz in the higher gap and then at the frequency $f=0.6284$ GHz in the lower gap [Fig. 2(c)]. We display the computed displacements in the (x and y) plane for a section in the middle of the plate ($z=e/2$). It is clearly seen that in both cases the incident wave propagates without attenuation and with a strong confinement inside the waveguide. Only a slight amount of energy leaks out of the waveguide.

The dispersion of the waveguide structure with $w_g=1.2$ μm is shown in Fig. 3(a). In this diagram, the red

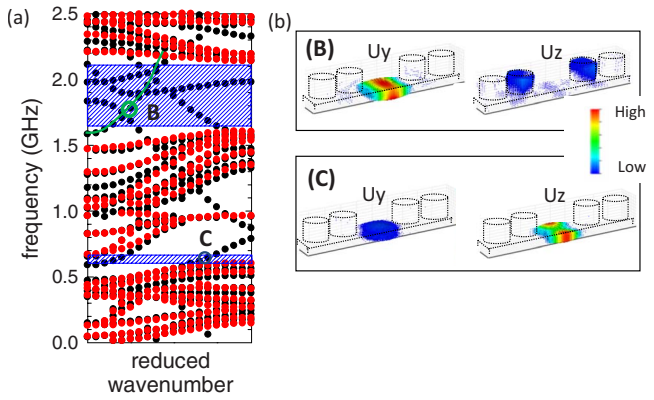

FIG. 3. (Color online) (a) Dispersion curves of the perfect phononic crystal (red dots) and for the line-defect waveguide structure for a five lattices parameters unit cells in the ΓX direction of the Brillouin zone (black dots). (b) 3D eigenmode representation at the points B ($ka/\pi=0.26$ and $f=1.778$ GHz) and C ($ka/\pi=0.737$ and $f=0.6426$ GHz) for the two polarizations, parallel (U_y) and perpendicular (U_z) to the plate. The blue (red) color corresponds to the lower (higher) value of the displacement field modulus while the white color corresponds to a displacement equal to zero but does not appears in the color bar.

dots represent the band structure of the perfect phononic crystal for a supercell of five periods and the black dots the band structure with the linear waveguide. In this latter case, we can observe several modes inside both the low- and high-frequency gaps, which correspond to the existence of defect modes confined in the waveguide. Nevertheless, when comparing with the transmission spectrum, it seems that many of these branches do not contribute to the transmission of the incident longitudinal waves. We made a complete analysis of the eigenmodes for different branches and found that, in the higher gap, only one branch has the appropriate longitudinal polarization in order to efficiently contribute to the transmission. The displacement field of this mode was calculated for a reduced wave number $ka/\pi=0.26$ and frequency $f=1.778$ GHz [point B in Fig. 3(a)] and is presented in Fig. 3(b). The wave is well localized within the waveguide and essentially exhibits a longitudinal displacement U_y whereas the normal component U_z is almost equal to zero. For the low-frequency gap, there are two localized branches existing at low and high wave vectors, respectively. For the branch at low wave vector, the polarization is mainly U_x and does not contribute to the transmission. Figure 3(c) displays the displacement field in the second branch associated with the mode at the point C ($ka/\pi=0.737$ and $f=0.6426$ GHz). We can see that the mode is mainly polarized along z with a weak longitudinal contribution along U_y. From this analysis, we can understand that the branch at higher wave vectors contributes to a transmission perpendicular to the plate. These conclusions are in accordance with the transmission spectra shown in Fig. 2.

As a summary, the transmission of a longitudinal incident pulse through a conventional waveguide gives rise to a mainly longitudinal wave in the range of the high-frequency gap while a conversion to a wave with a normal component to the plate occurs in the low-frequency gap.

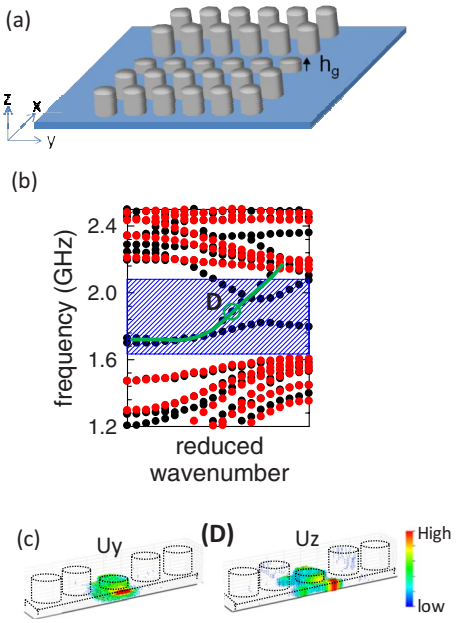

FIG. 4. (Color online) (a) Schematic view of a linear waveguide made of dots of different height h_g. (b) Black dots: dispersion curves for a waveguide structure of height $h_g=0.2$ μm in the high-frequency range. (c) Eigenmode representation at the point D ($ka/\pi=0.58$ and $f=1.885$ GHz) for U_y and U_z. The blue (red) color corresponds to the lower (higher) value of the displacement field modulus while the white color corresponds to a displacement equal to zero but does not appears in the color bar.

B. Linear waveguide made up of dots of different height

In this section, we study a waveguide structure obtained by changing the height of the dots along one row. We show, more especially, the case where the height h_g [Fig. 4(a)] is smaller than that in the perfect crystal and is in a scale ranging from 0.6 to 0.1 μm. The band-structure analysis reveals that, when $h_g \leq 0.4$ μm, new localized modes appear inside the gaps. Those defect branches shift toward the higher frequencies as far as the height of the dots decreases.

Figure 4(b) displays the dispersion curves magnified in the frequency range [1.2 and 2.5 GHz]. In this figure, the black dots represent the band structure of the linear waveguide ($h=0.2$ μm) compared with the band structure of the perfect phononic crystal ($h=0.6$ μm) represented by the red dots. We can observe three guided modes inside the high-frequency gap, among them we especially focus on the branch, which crosses the whole frequency range of the gap. Figure 4(c) presents the eigenmode corresponding to the point D ($ka/\pi=0.58$ and $f=1.885$ GHz) on this branch. We can observe that both components U_y and U_z of the displacement field are represented and strongly localized within the dot constituting the waveguide. In Fig. 5(a), we present, for the incident longitudinal pulse, the transmission coefficients for the components U_y and U_z of the displacement field and observe a similar magnitude of both components in the transmitted waves. In this figure, the length of the waveguide is assumed to be seven periods which is sufficient to have a sharp drop of the transmission coefficient at the edges of the gap. To complete the study, the propagation and confinement

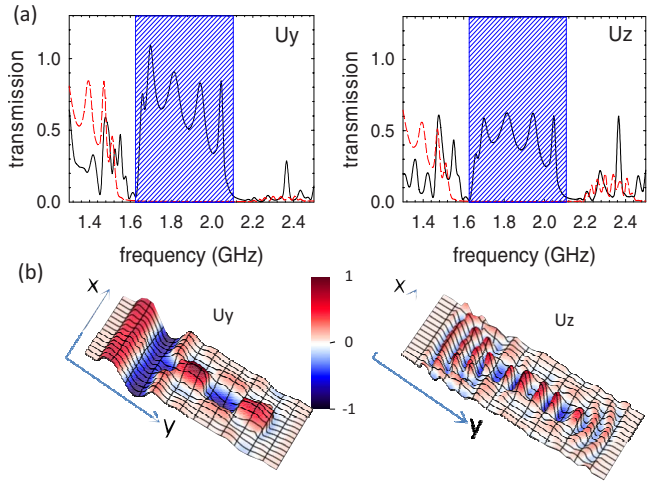

FIG. 5. (Color online) (a) Transmission spectrum for the waveguide structure of Fig. 4(a) for h_g=0.2 μm according to the U_y and U_z polarizations. The length of the phononic crystal is seven periods. (b) Displacement field distributions in the (x and y) plane at the thickness $z=e/2$ for the U_y and U_z polarizations at the monochromatic frequency f=1.698 GHz. The red (blue) color represents the positive (negative) contribution of the wave.

of the acoustic waves are represented using a displacement field representation for the components U_y and U_z at the incident monochromatic frequency f=1.698 GHz [Fig. 5(b)].

Figure 6(a) displays the dispersion curves and the corresponding transmission spectra in the low-frequency range [0.3 and 0.8 GHz] for h_g=0.3 μm. The value of h_g is chosen

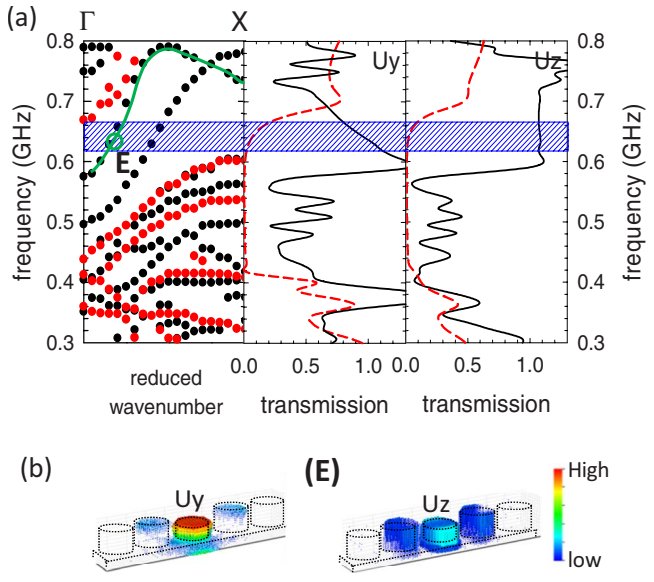

FIG. 6. (Color online) (a) Left: dispersion curves in the low-frequency range for the waveguide structure of Fig. 4(a) with a height h_g=0.3 μm (black dots). Right: corresponding transmission spectra for the U_y and U_z components. (b) Eigenmode analysis at the point E (ka/π=0.16 and f=0.6277 GHz) for (U_y) and (U_z). The blue (red) color corresponds to the lower (higher) value of the displacement field modulus while the white color corresponds to a displacement equal to zero but does not appears in the color bar.

in a way so that we obtain guided modes in the low-frequency gap extending from 0.4147 to 0.668 GHz along the ΓX direction. Nevertheless, we notice that this gap is much wider than the absolute band gap because the lower limit of the band gap along ΓM direction is 0.613 GHz. This effect explains the existence of several peaks of transmission inside the ΓX partial band gap [0.4147 and 0.613 GHz], which correspond to acoustic waves leaking out of the waveguide toward the ΓM direction. Therefore, this frequency region is not very useful for guiding of confined modes. In the frequency range of the absolute band gap (red shaded area), there is a transmitted signal around the frequency 0.6277 GHz for both U_y and U_z, with a higher transmission coefficient for the longitudinal polarization. The corresponding band diagram shows two confined branches. The branch, which crosses the whole gap, has an U_x polarization and does not contribute to the transmission. For the other branch, the eigenmode at point E (ka/π=0.16 and f=0.6277 GHz) is sketched in Fig. 6(b). This mode is mainly polarized along y but is again with a non-negligible component along z. The first of these components is strongly localized inside the guiding dots while the latter is less confined and penetrates over the dots in the neighborhood of the waveguide. Therefore, a good correspondence between the band diagram and transmitted curve is obtained.

To summarize this section, the waveguide created by decreasing the height of the cylinders can transmit confined modes inside both the high- and low-frequency band gaps. In the former case, the incident longitudinal wave gives rise to transmitted waves with components both parallel and perpendicular to the plates. In the latter case, the transmitted wave has a main longitudinal component but also a smaller normal component with a weaker confinement inside the waveguide. A similar study can be performed if the height of the cylinders is increased with respect to the one in the perfect crystal.

C. Linear waveguide made up of dots of different material

In this section, we assume that the waveguide is formed from a row of dots made up of a different material than those in the perfect crystal [Fig. 7(a)]. We chose cylinders made up of Si and Al in the waveguide to obtain propagation in the higher and lower gaps, respectively.

In Fig. 7(b), we show, in the frequency range [1.4 and 2.5 GHz], both dispersion curves and transmission of U_y and U_z components of the displacement field when the dots in the guide are made up of Si. We can observe that the transmitted waves contain both components. Among the three dispersion curves existing in the band gaps, two have an U_x polarization and should not contribute to the transmission. Only in one branch the displacement field has U_y and U_z components as illustrated for the point F situated at the wave number ka/π=0.37 and frequency f=1.777 GHz. This is the only branch contributing to the transmission.

Similarly, we report, in Fig. 8, the case of a waveguide made up of aluminum dots, which is well adapted for the propagating signal in the low-frequency gap. Here, the interesting point is to have only one localized mode appearing in

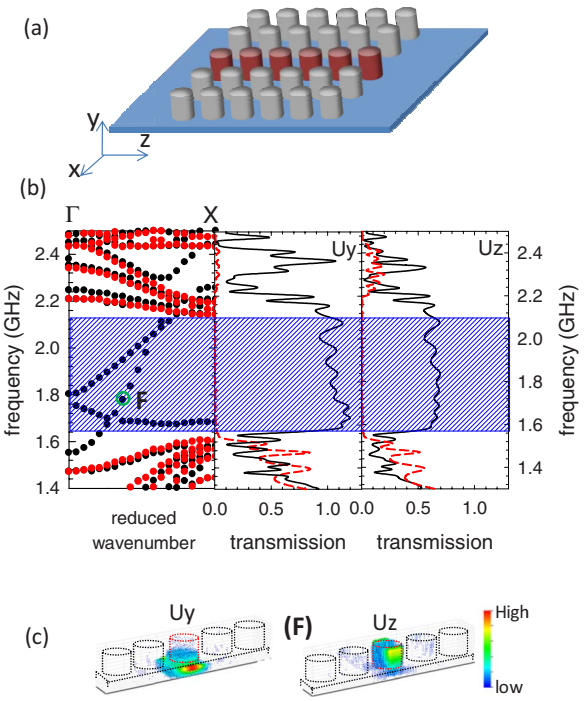

FIG. 7. (Color online) (a) Schematic view of a linear waveguide made of different material dots symbolized in red. (b) Left: dispersion curves in the high-frequency regime for silicon inserted dots forming the waveguide. Middle and right: corresponding transmission spectrum for the both components U_y and U_z. The length of the phononic crystal is ten periods. (c) U_y and U_z eigenmode calculations at the point F ($ka/\pi=0.37$ and $f=1.777$ GHz). The blue (red) color corresponds to the lower (higher) value of the displacement field modulus while the white color corresponds to a displacement equal to zero but does not appears in the color bar.

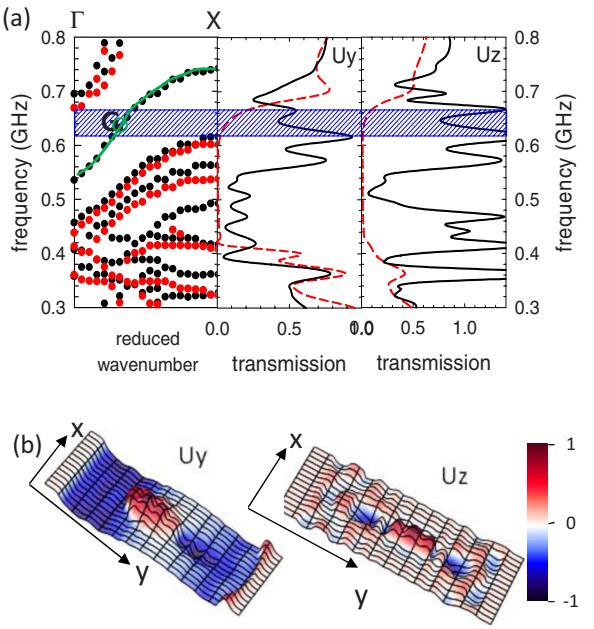

FIG. 8. (Color online) (a) Left: dispersion curves in the low-frequency regime for aluminum dots forming the waveguide. Middle and right: corresponding transmission spectrum for the both components U_y and U_z. The length of the phononic crystal is seven periods. (b) Displacement field distribution in the (x and y) plane at the thickness $z=e/2$ for the U_y and U_z polarizations at the monochromatic frequency $f=0.6311$ GHz.The red (blue) color represents the positive (negative) contribution of the wave.

the gap [Fig. 8(a)] giving rise to a monomode waveguide. The transmitted waves contain U_y and U_z components of the displacement field. This conclusion is supported by the map of the propagating confined field in the waveguide [Fig. 8(b)] at the frequency $f=0.6311$ GHz. It is worthy to remind that, here, the wavelength of the wave transmitted through the guide is more than ten times larger than the lattice parameter of the phononic crystal. As a result, a waveguide whose length is ten unit cells of the phononic crystal contains less than one period of the confined mode.

IV. CONCLUSIONS

We developed a FDTD method to analyze phonon transport and waveguiding though a phononic crystal made up of cylindrical dots deposited on a thin homogeneous plate. With an appropriate choice of the physical and geometrical parameters, existence of two absolute band gaps is ensured. The first is in a frequency range where all wavelengths in the silicon membrane are about ten times larger than the period of the phononic crystal. The second falls in the Bragg frequency regime. We showed that there is a good correspondence between the transmission spectrum and dispersion curves. Using both transmission and dispersion phonon calculations, we studied propagation of the symmetric longitudinal Lamb wave S_0 through linear waveguides obtained either by removing a row of dots or changing the nature or the geometrical parameters of the dots in a row. In the first case, the polarization of the transmitted wave remains mainly longitudinal in the higher band gap while a conversion to the normal polarization occurs in the lower band gaps. When the waveguide is obtained by changing the height of the dots in a row, the transmitted wave contains both components of the displacement field in the frequency range of the higher as well as the lower gap. However, in the second, confinement is better ensured for the longitudinal component. Finally, the transmission can also be achieved through a waveguide where the material constituting the dots is different from the one in the perfect phononic crystal. The transmitted waves travel with a good confinement in the guide and contain both component of the displacement field. The advantage of this case is to limit the number of defect modes inside each band gap, which could be more suitable for filtering applications. Results presented in this paper could be applied to the innovative design of acoustic-wave devices for wireless applications.

ACKNOWLEDGMENT

This work was supported (in part) by the European Commission (EC) Seventh Framework program (FP7) under the (IP) Project Reference No. 216176 (NANOPACK, www.nanopack.org).

*Corresponding author; yan.pennec@univ-lille1.fr

[1] For a review, see M. S. Kushwaha, Recent Res. Dev. Appl. Phys. **2**, 743 (1999).
[2] M. S. Kushwaha, P. Halevi, L. Dobrzynski, and B. Djafari-Rouhani, Phys. Rev. Lett. **71**, 2022 (1993).
[3] M. M. Sigalas and E. N. Economou, Solid State Commun. **86**, 141 (1993).
[4] F. R. Montero de Espinosa, E. Jiménez, and M. Torres, Phys. Rev. Lett. **80**, 1208 (1998).
[5] J. V. Sánchez-Pérez, D. Caballero, R. Mártinez-Sala, C. Rubio, J. Sánchez-Dehesa, F. Meseguer, J. Llinares, and F. Gálvez, Phys. Rev. Lett. **80**, 5325 (1998).
[6] M. Torres, F. R. Montero de Espinosa, D. Garcia-Pablos, and N. Garcia, Phys. Rev. Lett. **82**, 3054 (1999).
[7] M. Kafesaki, M. M. Sigalas, and N. Garcia, Phys. Rev. Lett. **85**, 4044 (2000); Physica B **296**, 190 (2001).
[8] A. Khelif, B. Djafari-Rouhani, J. O. Vasseur, and P. A. Deymier, Phys. Rev. B **68**, 024302 (2003).
[9] Y. Pennec, B. Djafari-Rouhani, J. O. Vasseur, A. Khelif, and P. A. Deymier, Phys. Rev. E **69**, 046608 (2004).
[10] Y. Pennec, B. Djafari-Rouhani, J. O. Vasseur, H. Larabi, A. Khelif, A. Choujaa, S. Benchabane, and V. Laude, Appl. Phys. Lett. **87**, 261912 (2005).
[11] Z. Liu, X. Zhang, Y. Mao, Y. Y. Zhu, Z. Yang, C. T. Chan, and P. Sheng, Science **289**, 1734 (2000).
[12] Ph. Lambin, A. Khelif, J. O. Vasseur, L. Dobrzynski, and B. Djafari-Rouhani, Phys. Rev. E **63**, 066605 (2001).
[13] C. Goffaux, J. Sánchez-Dehesa, A. Levy Yeyati, Ph. Lambin, A. Khelif, J. O. Vasseur, and B. Djafari-Rouhani, Phys. Rev. Lett. **88**, 225502 (2002).
[14] M. Hirsekorn, Appl. Phys. Lett. **84**, 3364 (2004).
[15] Y. A. Kosevich, C. Goffaux, and J. Sanchez-Dehesa, Phys. Rev. B **74**, 012301 (2006).
[16] H. Larabi, Y. Pennec, B. Djafari-Rouhani, and J. O. Vasseur, Phys. Rev. E **75**, 066601 (2007).
[17] Y. Tanaka and S. I. Tamura, Phys. Rev. B **58**, 7958 (1998).
[18] Y. Tanaka and S. I. Tamura, Phys. Rev. B **60**, 13294 (1999).
[19] T. T. Wu, Z. G. Huang, and S. Lin, Phys. Rev. B **69**, 094301 (2004).
[20] V. Laude, M. Wilm, S. Benchabane, and A. Khelif, Phys. Rev. E **71**, 036607 (2005).
[21] J. H. Sun and T. T. Wu, Phys. Rev. B **74**, 174305 (2006).
[22] J. J. Chen, K. W. Zhang, J. Gao, and J. C. Cheng, Phys. Rev. B **73**, 094307 (2006).
[23] J. J. Chen, H. L. W. Chan, and J. C. Cheng, Phys. Lett. A **366**, 493 (2007).
[24] J. Gao, X. Y. Zou, J. C. Cheng, and B. W. Li, Appl. Phys. Lett. **92**, 023510 (2008).
[25] J. O. Vasseur, P. A. Deymier, B. Djafari-Rouhani, and Y. Pennec, Proceedings of IMECE 2006, ASME International Mechanical Engineering Congress and Exhibition, Chicago, Illinois, 5–10 November 2006, pp. 125–133.
[26] J. C. Hsu and T. T. Wu, Phys. Rev. B **74**, 144303 (2006).
[27] A. Khelif, B. Aoubiza, S. Mohammadi, A. Adibi, and V. Laude, Phys. Rev. E **74**, 046610 (2006).
[28] J. O. Vasseur, A. C. Hladky-Hennion, B. Djafari-Rouhani, F. Duval, B. Dubus, and Y. Pennec, J. Appl. Phys. **101**, 114904 (2007).
[29] J. C. Hsu and T. T. Wu, Appl. Phys. Lett. **90**, 201904 (2007).
[30] J. O. Vasseur, P. A. Deymier, B. Djafari-Rouhani, Y. Pennec, and A. C. Hladky-Hennion, Phys. Rev. B **77**, 085415 (2008).
[31] J. H. Sun and T. T. Wu, Phys. Rev. B **76**, 104304 (2007).
[32] J. F. Robillard, A. Devos, and I. Roch-Jeune, Phys. Rev. B **76**, 092301 (2007).
[33] C. Giannetti, B. Revaz, F. Banfi, M. Montagnese, G. Ferrini, F. Cilento, S. Maccalli, P. Vavassori, G. Oliviero, E. Bontempi, L. E. Depero, V. Metlushko, and F. Parmigiani, Phys. Rev. B **76**, 125413 (2007).
[34] A. Sato, Y. Pennec, B. Djafari-Rouhani, G. Fytas, W. Knoll, and M. Steinhart, J. Chem. Phys. **130**, 111102 (2009).
[35] Y. Pennec, B. Djafari-Rouhani, H. Larabi, J. O. Vasseur, and A. C. Hladky-Hennion, Phys. Rev. B **78**, 104105 (2008).
[36] T. T. Wu, Z. G. Huang, T.-C. Tsai, and T. C. Wu, Appl. Phys. Lett. **93**, 111902 (2008).
[37] T. C. Wu, T. T. Wu, and J. C. Hsu, Phys. Rev. B **79**, 104306 (2009).
[38] R. Chen, A. I. Hochbaum, P. Murphy, J. Moore, P. Yang, and A. Majumdar, Phys. Rev. Lett. **101**, 105501 (2008).
[39] J. N. Gillet, Y. Chalopin, and S. Volz, ASME J. Heat Transfer **131**, 043206 (2009); Y. Chalopin, J. N. Gillet, and S. Volz, Phys. Rev. B **77**, 233309 (2008).
[40] Y. Tanaka, Y. Tomoyasu, and S. I. Tamura, Phys. Rev. B **62**, 7387 (2000).